Soft Matter

PAPER

View Article Online
View Journal | View Issue

Check for updates

Cite this: *Soft Matter*, 2025, **21**, 6452

Received 28th March 2025,
Accepted 24th July 2025

DOI: 10.1039/d5sm00325c

rsc.li/soft-matter-journal

Osmocapillary phase separation at contact lines†

Qihan Liu * and Luochang Wang

Swollen soft materials have various uncommon wetting properties, such as anomalous contact angles, extremely low adhesion, stimuli-responsive adhesion, and time-dependent wetting. These properties are related to the solvent exudation near the contact lines. Existing studies assume that the phenomenon is governed by the elastocapillary effect, predicting that a stiffer material suppresses the solvent exudation. Here we show that the phenomenon is governed by the osmocapillary effect instead, predicting that a stiffer material promotes solvent exudation while a higher osmotic pressure suppresses it. We combine a small-deformation analytical model and nonlinear finite element simulations to develop a model that quantitatively predicts a wide range of existing experimental data with no fitting parameters.

Open Access Article. Published on 25 July 2025. Downloaded on 4/4/2026 1:35:03 PM.
This article is licensed under a Creative Commons Attribution-NonCommercial 3.0 Unported Licence.

1. Introduction

Wetting is crucial for various industrial applications such as bonding,[1] lubrication,[2] coating,[3] and deicing.[4] Wetting on swollen soft materials, such as hydrogel, swollen rubber, and soaked fibrous and porous materials, often exhibits unique properties due to the solvent on the material surface. Here the solvent refers to the liquid that swells the material, such as water in a hydrogel, or uncrosslinked silicone polymer in a silicone elastomer. Examples include anomalous contact angle,[5,6] extremely low adhesion,[7,8] stimuli-responsive adhesion,[9,10] and time-dependent wetting.[11,12] Existing studies show that the solvent on the material surface is pulled out from the swollen solid near the contact line (Fig. 1A).[5,6] This phenomenon is often modeled as an elastocapillary effect,[5,6,12–14] *i.e.* the formation of the solvent phase is driven by surface tension and limited by the elasticity of the swollen solid. Under this picture, a stiffer solid would lead to a smaller solvent phase. Here we show that the phenomenon is governed by a different mechanism, osmocapillary phase separation.[15–18] Osmocapillary phase separation is still driven by the surface tension but is limited by osmotic pressure instead of elasticity. Under this picture, the stiffness of the solid plays a secondary role in determining the size of the solvent phase; and a stiffer solid will increase the size of phase separation rather than decrease it. This new picture has significant implications for the design of future related studies.

Osmocapillary theory assumes that the solvent on a swollen solid surface is a phase separation caused by the competition between capillarity and osmosis.[15] The solvent molecules on the surface and in the solid must be in thermodynamic equilibrium, thus having the same chemical potential $\mu = \mu_0 - \Omega\Pi$. Here μ_0 is the chemical potential of the solvent molecule at the ambient condition; Ω is the average volume per solvent molecule; and Π is the osmotic pressure of the swollen solid. Here the osmotic pressure Π may come from the free energy of mixing between a polymer network and a solvent, or the capillary action of a fibrous or porous matrix. In the latter case, Π is equivalent to pore pressure but with an opposite sign. The thermodynamic equilibrium implies that the solvent phase separation is under a uniform tension of Π. On the boundaries of the solvent phase, the surface tension generates Laplace pressure $\gamma\kappa$, where γ is the interfacial tension and κ is the sum of the local curvatures. The morphology of the solvent phase is governed by the balance between osmotic pressure and the Laplace pressure.

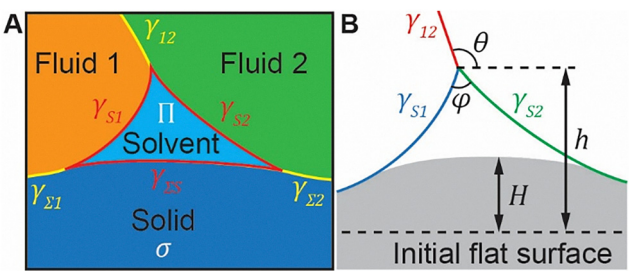

Fig. 1 (A) The osmocapillary phase separation near the contact line is governed by the force balance between the osmotic pressure Π in the solvent, the interfacial tension γ between different phases, and the elastic stress σ in the solid. The subscripts Σ,S,1,2 indicate solid, solvent, fluid 1, and fluid 2. (B) An example simulation with $\gamma_{12}/\gamma_{tot} = 0.86$ where $\gamma_{tot} = \gamma_{S1}/\gamma_{S2}$, $\gamma_{S2}/\gamma_{S1} = 2$, $\Pi/G = 1$. The solid height H, solvent height h, (both relative to the initial flat surface), apparent contact angle θ, and the tip angle φ are used to characterize the equilibrium configuration of the phase separation.

Department of Mechanical Engineering and Materials Science, University of Pittsburgh, Pittsburgh, PA 15261, USA. E-mail: qihan.liu@pitt.edu

† Electronic supplementary information (ESI) available. See DOI: https://doi.org/10.1039/d5sm00325c

This journal is © The Royal Society of Chemistry 2025

Open Access Article. Published on 25 July 2025. Downloaded on 4/4/2026 1:35:03 PM. This article is licensed under a Creative Commons Attribution-NonCommercial 3.0 Unported Licence.

2. Numerical and analytical modeling

Consider the contact between two fluids and a swollen solid (Fig. 1A). The solvent and the two fluids are mutually immiscible. For example, the two fluids can be air and water while the solid is silicone elastomer swollen in silicone oil. At equilibrium, the two fluids are stress-free and the solvent is under uniform hydrostatic tension Π. These three liquid phases do not require explicit modeling. We only need to model the stress balance inside the solid and the following force balance conditions at the phase boundaries:

1. At the solvent–fluid interfaces, the osmotic pressure Π is balanced by the Laplace pressure: $\Pi = \gamma_{S1}\kappa$ or $\Pi = \gamma_{S2}\kappa$. γ_{S1} or γ_{S2} is the interfacial tension between the solvent and the fluid 1 or 2. κ is the sum of the local principal curvature.

2. At the solid–fluid boundaries, the elastic stress σ is balanced by the Laplace pressure: $\sigma = \gamma_{\Sigma 1}\kappa$ or $\sigma = \gamma_{\Sigma 2}\kappa$. $\gamma_{\Sigma 1}$ or $\gamma_{\Sigma 2}$ is the interfacial tension between the swollen solid and the fluid 1 or 2.

3. At the solvent–solid boundary, the elastic stress σ is balanced by both the Laplace pressure from the solid–solvent interface and the osmotic pressure in the solvent: $\sigma = \gamma_{\Sigma S}\kappa + \Pi$. $\gamma_{\Sigma S}$ is the solid–solvent interfacial tension.

4. Any of the three-phase contact lines between the solid, solvent, and the two fluids must follow the Neumann's law requiring that the force balance between the three interfacial tensions.[19,20]

The boundary value problem outlined above can be readily implemented in finite element analysis by modeling the interfaces as a layer of shell elements in 3D or beam elements in 2D.[18,21] The interfacial tension is implemented as pre-stress in the shell or beam layers. To ensure that the interfacial tension is deformation-independent, the tensile stiffness of the shell or beam must be sufficiently low. The solid interfaces are allowed to frictionlessly slide on the solid but not penetrate or detach from it. The fluid interfaces are allowed to move freely in space but not penetrate the solid. This implementation automatically produces the correct Laplace pressure and ensures the force balance at the contact lines. A uniform pressure Π towards the direction of phase separation is applied on all the solvent interfaces to represent osmotic pressure.

We implement this algorithm for a simplified problem (Section S1, ESI†). Here we study the contact angle of a fluid droplet on a flat swollen solid with the following simplifications:

1. The solid is much larger than the size of the osmocapillary phase separation. Then the dimension and the far-field boundary conditions of the simulation negligibly affect the result.

2. The fluid droplet is much larger than the size of the osmocapillary phase separation. Then the deformation near the contact line is 2D plane strain. Also, the interface between the two fluids will be flat (Fig. 1B red interface), the orientation of which can be determined by Neumann's law without simulating this interface.

3. The swollen solid and the solvent have indistinguishable surface properties: $\gamma_{\Sigma 1} = \gamma_{S1}$, $\gamma_{\Sigma 2} = \gamma_{S2}$, and $\gamma_{\Sigma S} = 0$. This is valid for highly swollen gels where the solvent occupies a high volume fraction,[22] or systems where the solid and the solvent are chemically similar thus having similar surface energies, such as silicone elastomer swollen in silicone oil.[6] In this case, we only need to model the two interfaces (Fig. 3B blue and green interfaces). Each interface represents the solid–fluid interfaces when in contact with the solid and the solvent–fluid interfaces when detached from the solid.

4. The solid follows the incompressible neo-Hookean model, which represents the behavior of polymer networks. Note that swellable polymer networks can have large volume changes, thus being compressible, when connected to an environmental source of the solvent. However, in the absence of an environmental source, shear deformation is much easier than the volumetric deformation, thus effectively incompressible, for most swelling ratios according to the Flory–Rehner model.[18]

With these simplifications, the simulation is governed by three dimensionless groups: γ_{12}/γ_{tot} with $\gamma_{tot} = \gamma_{S1} + \gamma_{S2}$, γ_{S2}/γ_{S1}, and Π/G with G the shear modulus of the swollen solid. Here γ_{12}/γ_{tot} characterizes the competition between fluid interfacial tension γ_{12} that tends to pull the solvent surface up and the solvent interfacial tension γ_{tot} that tends to maintain a flat solvent surface. γ_{S2}/γ_{S1} characterizes the asymmetry of the solid interfacial tension when in contact with different fluids. Π/G characterizes the competition between osmotic pressure that tends to deform the solid and elasticity that resists the deformation. We characterize the equilibrium configuration with four experimentally measurable quantities: the maximum heights of the deformed solid H and the solvent h relative to the undeformed initial surface, the apparent contact angle of the fluid–fluid interface θ, and the tip angel of the solvent φ (Fig. 1B). $\Delta h = h - H$ is taken an evaluation of the size of the phase separation.

In addition to the general finite element model, an analytical solution can be found when the deformation of the solid is linear (Section S2, ESI†). The assumption of linear deformation will be valid when the osmotic pressure is small compared to the modulus of the solid, *i.e.* $\Pi/G \ll 1$, then the osmotic pressure cannot significantly deform the solid. For $\Pi/G \sim 1$ or larger, significant deviation between the nonlinear finite element simulation and the analytical solution are expected. The analytical solution predicts:

$$\cos\theta = \frac{\gamma_{S1} - \gamma_{S2}}{\gamma_{12}}, \tag{1}$$

$$\varphi = 180^\circ - \alpha - \beta, \tag{2}$$

$$\Delta h = \frac{\gamma_{S1}}{\Pi}(1 - \cos\alpha) - \ln 2\frac{\gamma_{S1}\sin\alpha + \gamma_{S2}\sin\beta}{2\pi G}, \tag{3}$$

$$H = \frac{\gamma_{S1}\sin\alpha + \gamma_{S2}\sin\beta}{2\pi G}\left[1 + \ln\left(\frac{2x_0\Pi}{\gamma_{S1}\sin\alpha + \gamma_{S2}\sin\beta}\right)\right]. \tag{4}$$

Here eqn (1) for the apparent contact angle θ is identical to the classical Young's law for the contact angle.[19,20] Eqn (2) for the tip angle φ comes from the force balance at the solvent–fluid contact line, *i.e.* Neumann's law.[19,20] The meaning of the two auxiliary variables, $\alpha = \theta - \arccos\left[\left(\gamma_{12}^2 + {\gamma_{S1}}^2 - {\gamma_{S2}}^2\right)/2\gamma_{12}\gamma_{S1}\right]$

Open Access Article. Published on 25 July 2025. Downloaded on 4/4/2026 1:35:03 PM.
This article is licensed under a Creative Commons Attribution-NonCommercial 3.0 Unported Licence.

and $\beta = \arccos\left[-\left(\gamma_{12}^2 + {\gamma_{S2}}^2 - {\gamma_{S1}}^2\right)/2\gamma_{12}\gamma_{S2}\right] - \theta$, are discussed in Section S2 (ESI†). Eqn (3) for the phase separation size Δh has two parts: the first term is the size of osmocapillary phase separation assuming a flat solid surface. This term is independent of the elastic property of the solid. The second term is the deformation of the solid into the region of phase separation, which follows from the linear elastic solution of a uniform pressure distribution over a semi-infinite solid.[23] Eqn (4) for the solid height H follows the same linear elastic solution but accounts for the deformation outside the region of phase separation. x_0 is a parameter to match the far-field boundary condition with the asymptotic behavior solved in the semi-infinite domain. Eqn (3) shows that a stiffer solid (higher modulus G) increases the phase separation size Δh. This contrasts with the existing interpretation of the phenomenon, which suggests that Δh scales with the elastocapillary length, thus decreasing with the stiffness of the material.[5,6,12–14]

3. Results and discussion

We first study the cases of $\gamma_{12}/\gamma_{tot} \geq 1$. Then a force balance cannot be formed at the solvent–fluids contact line (recall Fig. 1B). The solvent will spontaneously spread onto the interface between fluid-1 and fluid-2, forming a thin interfacial layer.[24] In this case, the two solvent–fluid surfaces will be tangent at the top tip, resulting in a tip angle $\varphi = 0$, and the contact line configuration is equivalent to the case of $\gamma_{12}/\gamma_{tot} = 1$ and. We are left with two dimensionless groups γ_{S2}/γ_{S1} and Π/G, and three characterization quantities: the apparent contact angle θ, the solid height H, and the phase separation size Δh. By symmetry, we only need to study the cases of $\gamma_{S2}/\gamma_{S1} \geq 1$. H and Δh can be nondimensionalized by either of the two material length scales: elastocapillary length γ_{tot}/G or the osmocapillary length γ_{tot}/Π (Fig. 2). Depending on whether the shear modulus G or the osmotic pressure Π are used in the definition, these two length scales reflect the magnitudes of elastocapillary and the osmocapillary effects. We find that $\Delta h\Pi/\gamma_{tot} \sim 1$ and $HG/\gamma_{tot} \sim 1$ for any combination of Π/G and γ_{S2}/γ_{S1}. In contrast, $\Delta hG/\gamma_{tot}$ and $H\Pi/\gamma_{tot}$ vary by orders of magnitude. This suggests that the solid deformation is governed by the elastocapillary effect while the solvent phase separation is governed by the osmocapillary effect.

Then, we compare the simulated apparent contact angle θ, normalized phase separation size $\Delta h\gamma_{tot}/\Pi$, and normalized solid height $H\gamma_{tot}/G$ with the linear analytical model (eqn (1)–(4)) in Fig. 3. Here different normalizations are used for Δh and H according to the governing effects identified in Fig. 2. The analytical model agrees with the simulation in the limit of small Π/G, *i.e.* when the osmotic pressure cannot significantly deform the solid. An increase in the asymmetry of the solvent–fluid interfacial tension, γ_{S2}/γ_{S1}, results in a higher apparent contact angle θ (Fig. 3A). Then the fluid–fluid interfacial tension γ_{12} has a less vertical component to pull the solid or the solvent up, resulting in decreases in both the phase separation size Δh (Fig. 3B) and the solid height H (Fig. 3C). At high Π/G, however, the apparent contact angle θ increases from the constant values; the phase separation size Δh decreases and the solid height H increases less than the linear analytical model.

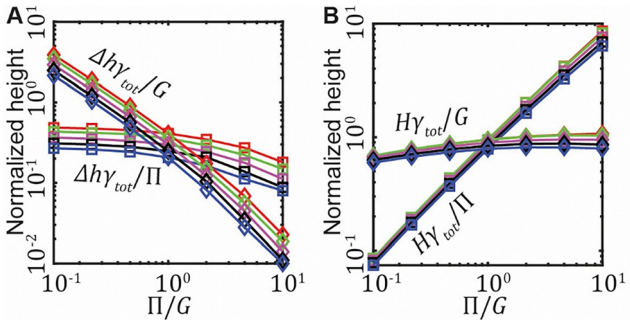

Fig. 2 (A) The osmocapillary length γ_{tot}/Π governs the phase separation size Δh. (B) The elastocapillary length γ_{tot}/G governs the solid height H red, green, magenta, black, and blue correspond to γ_{S2}/γ_{S1} = 1, 2, 3, 4, 5.

The deviations from the linear analytical model at large Π/G are caused by the nonlinear deformation illustrated in Fig. 3D. The linear analytical solution is accurate at low Π/G because the solid is negligibly deformed. As Π/G increases, the high osmotic pressure relative to shear modulus can significantly deform the solid. If we rescale the simulation under the constant osmocapillary length γ_{tot}/Π (Fig. 3D left column), we see that the solid gradually deforms into the region of phase separation, causing the solid height H to increase and the phase separation size Δh to decrease as predicted by the linear analytical model. However, as the solid deforms upward, the width of the phase separation decreases, reducing the total suction applied by the phase separation. Since the linear analytical model did not account for this change in the width of phase separation, it overestimates the solid deformation in Fig. 3B and C. Moreover, as the solid deforms into the region of phase separation, the bottom of the osmocapillary phase separation rotates towards the direction of the fluid–fluid interface (red dashed lines in Fig. 3D). This leads to the increase in θ observed in Fig. 3A. On the other hand, if we rescale the simulation under the constant elastocapillary length γ_{tot}/G (Fig. 3D right column), we see that the solid profile outside the region of phase separation is negligibly affected by Π/G. As Π/G increases, the size of phase separation becomes negligible and the surface profile approaches a purely elastocapillary ridge,[25,26] whose size is limited by the elastocapillary length. In fact, we observe that $H\gamma_{tot}/G$ approaches a limiting value of $H = 1.09\sin\theta\ \gamma_{tot}/G$ at high Π/G, as represented by the dashed lines in Fig. 3C.

Next, we study the cases of $\gamma_{12}/\gamma_{tot} < 1$, which will result in a finite tip angle φ according to the contact line force balance illustrated in Fig. 1B. It is found that eqn (1) (Young's law) decently predicts the apparent contact angle θ in all cases (Fig. 4A). Eqn (1) does underpredict θ for γ_{12}/γ_{tot} close to 1 and slightly overpredicts it for small γ_{12}/γ_{tot}, and the deviation increases with Π/G. This can be attributed to the rotation of the phase separation at high Π/G discussed in Fig. 3D. Eqn (2) (Neumann's law) perfectly predicts the tip angle φ independent

 This journal is © The Royal Society of Chemistry 2025

Open Access Article. Published on 25 July 2025. Downloaded on 4/4/2026 1:35:03 PM.
This article is licensed under a Creative Commons Attribution-NonCommercial 3.0 Unported Licence.

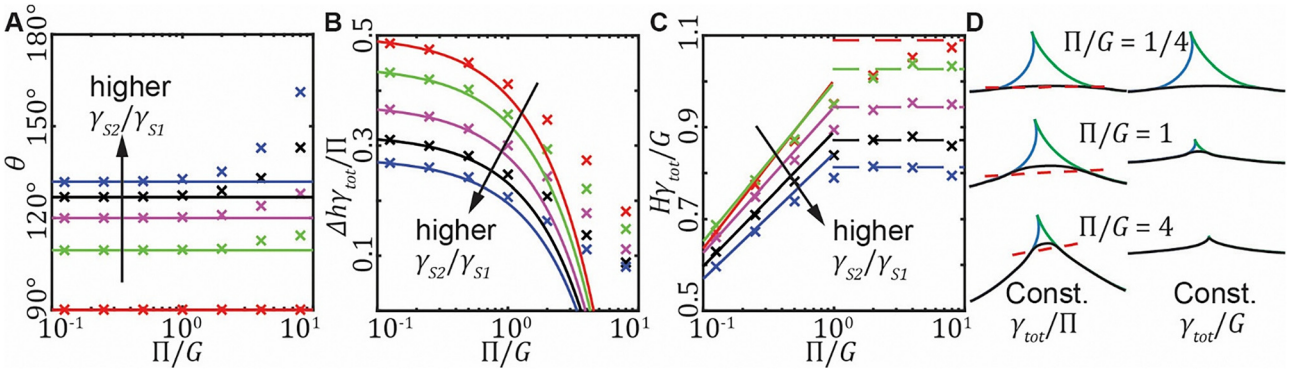

Fig. 3 In the limit of $\gamma_{12}/\gamma_{tot} = 1$, how Π/G and γ_{S2}/γ_{S1} affect (A) apparent contact angle θ, (B) phase separation size Δh, and (C) solid height H. Crosses are simulation results. Solid lines are the analytical solution (eqn (1)–(4)). The dashed lines in (C) are the limiting behavior $H = 1.09 \sin\theta\, \gamma_{tot}/G$. Red, green, magenta, black, and blue correspond to $\gamma_{S2}/\gamma_{S1} = 1, 2, 3, 4, 5$. (D) Sample surface profiles from nonlinear finite element simulation for $\gamma_{S2}/\gamma_{S1} = 2$ under different rescaling. Blue, green, and black lines represent the two solvent–fluid interfaces and the gel surface. The red dashed lines connect the solvent–fluid–solid contact lines to show the rotation of the phase separation.

of Π/G (Fig. 4B) because the local force balance at the solvent–fluids contact line is not affected by the deformation of the solid. The phase separation size Δh (Fig. 4C) and the solid height H (Fig. 4D) both reduce with γ_{12}/γ_{tot} because γ_{12} is the driving force that pulls the solvent and the solid upward. Eqn (3) underpredicts Δh and eqn (4) overpredicts H at large Π/G, consistent with the observations in Fig. 3B and C. The limiting behavior, $H = 1.09 \sin\theta\, \gamma_{tot}/G$, remains valid at large Π/G.

4. Experimental comparison

We compare our theoretical model with the experimental results by Cai *et al.*[6] The experiments characterized the contact between a water droplet and a piece of silicone gel in the air. Silicone gel, corresponding to the solid in this paper, is swollen in silicone oil so that the solvent and the solid have identical surface properties, identical to our assumption. Denote air as fluid 1 and water as fluid 2. Then, $\gamma_{12} = 72.2$ mN m^{-1}, $\gamma_{S1} = 19.7$ mN m^{-1}, $\gamma_{S2} = 43.2$ mN m^{-1}, corresponding to the cases of $\gamma_{12} \geq \gamma_{tot}$ where the solvent spreads onto the fluid interface. Cai *et al.* have directly measured θ, φ, h, and H using confocal microscopy. They have fitted the gel modulus using the scaling relation $G = G_0\phi^{0.56}$, where G_0 is the shear modulus of the dry network and ϕ is the polymer volume fraction at the swollen state. However, they did not measure the osmotic pressure Π Since Δh is governed by the osmocapillary effect and H is governed by the elastocapillary effect (recall Fig. 2), we use $\Delta h/H$ in lieu of Π/G to compare the experimental results with the theoretical model. This approach is supported by the simulation results showing that $\Delta h/H$ monotonic decreases with Π/G (Fig. S4, ESI†), then any functional dependence on Π/G can be one-to-one mapped onto $\Delta h/H$.

The experimental data show that the apparent contact angle θ increases with Π/G while the tip angle φ remains constant, qualitatively agreeing with our results. However, the exact value does not match, likely due to the limited resolution of the imaging technique near the contact line (Section S3, ESI†).

The experimental data also show that the phase separation size Δh increases with swelling yet the solid deformation H decreases with swelling. Since swelling reduces the ratio Π/G, this observation again qualitatively agrees with our results in Fig. 3B and C. To quantitatively compare with the observed solid and liquid heights, H and h, over a wide range of Π/G, we

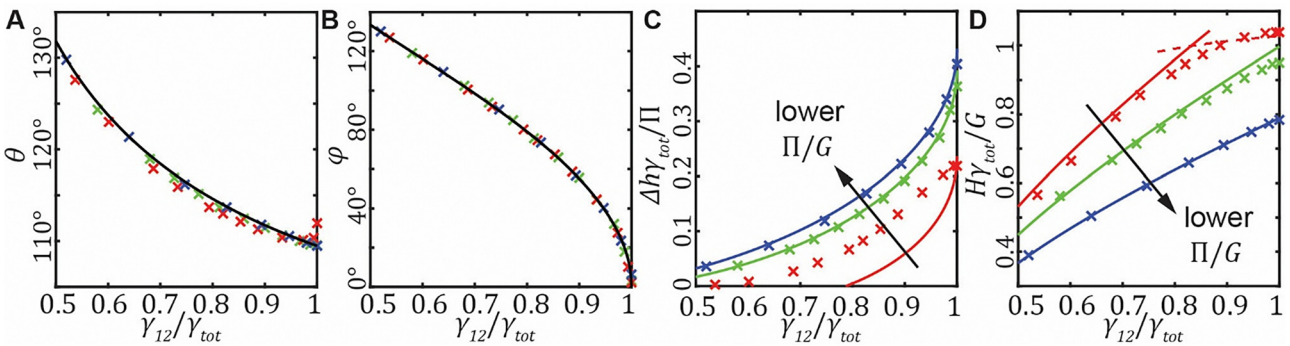

Fig. 4 With $\gamma_{S2}/\gamma_{S1} = 2$, how γ_{12}/γ_{tot} and Π/G affect (A) apparent contact angle θ, (B) tip angle φ, (C) phase separation size Δh, and (D) solid height H. Crosses are simulation results. Solid lines are the analytical solution. The dashed line in (D) is the limiting behavior $H = 1.09 \sin\theta\, \gamma_{tot}/G$. Red, green, and blue correspond to $\Pi/G = 4, 1, 0.25$.

Open Access Article. Published on 25 July 2025. Downloaded on 4/4/2026 1:35:03 PM.
This article is licensed under a Creative Commons Attribution-NonCommercial 3.0 Unported Licence.

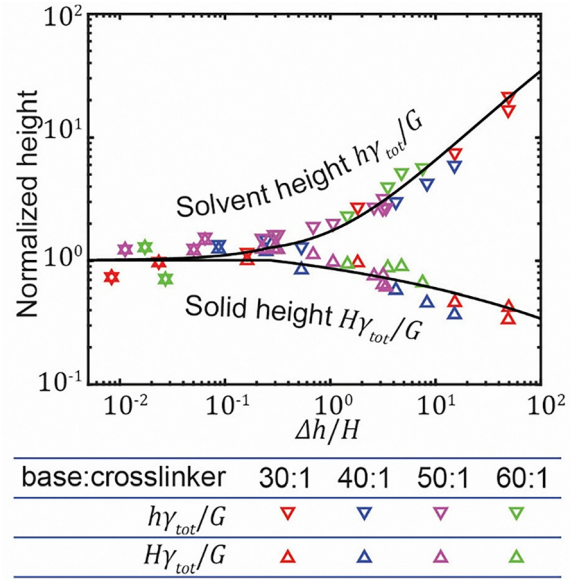

Fig. 5 Compare theory with the data by Cai *et al.*[6] Lower base: crosslinker ratio corresponds to a stiffer gel.

use the limiting behaviors identified through the nonlinear finite element simulation to correct the linear analytical model, eqn (3) and (4):

1. If eqn (3) predicts negative phase separation size $\Delta h < 0$, set $\Delta h = 0$ because physically this size cannot be negative.

2. If eqn (4) predicts a solid deformation H exceeding the elastocapillary limit, set it to the limiting value $H = 1.09 \sin\theta\, \gamma_{tot}/G$.

We have verified that the linear analytical solution with these two corrections can decently represent our simulation results (Fig. S5, ESI†). Using the silicone oil–air interfacial tension γ_{S_1} and silicone oil–water interfacial tension γ_{S_2} as the only input parameters, the modified model can perfectly predict the experimental measurement with no fitting parameter (Fig. 5).

5. Conclusion

In conclusion, we have shown that the solvent near a contact line is osmocapillary phase separation, distinct from the commonly studied elastocapillary deformation. The size of the phase separation Δh is governed by the osmocapillary length γ_{tot}/Π and gradually decreases with the dimensionless ratio between osmotic pressure and shear modulus, Π/G, and the asymmetry of the solvent–fluid interfacial tensions, γ_{S2}/γ_{S1}. This is contrary to the common belief that the phase separation size Δh decreases with the stiffness of the material G. People observed smaller Δh with higher G simply because a dryer polymer network has both a higher Π/G and a higher G.[15] This suggests the need to independently monitor the osmotic pressure Π in future studies. We also show that the apparent contact angle θ increases with Π/G. Since deformation can affect Π, this can lead to deformation-dependent contact angle, a feature that was previously associated with deformation-dependent surface energy.[25] This suggests the need to carefully check for the osmocapillary phase separation when studying the contact angle on elastomers.

Conflicts of interest

There are no conflicts to declare.

Data availability

The work did not generate any data. Necessary information to reproduce the simulation in the commercial software ABAQUS has been included in the ESI.†

Acknowledgements

This material is based upon work supported by National Science Foundation under grant no. 2337592. Any opinions, findings, and conclusions or recommendations expressed in this material are those of the author(s) and do not necessarily reflect the views of the National Science Foundation. The author thanks Dr Jonathan T. Pham for sharing the experimental data and helpful discussion on data interpretation.

References

1 A. V. Pocius, *Adhesion and adhesives technology: an introduction*, Carl Hanser Verlag GmbH Co KG, 2021.
2 M. Kalin and M. Polajnar, *Tribol. Lett.*, 2013, **52**, 185.
3 L. Scriven, *MRS Online Proc. Libr.*, 1988, **121**, 717.
4 A. Dotan, H. Dodiuk, C. Laforte and S. Kenig, *J. Adhes. Sci. Technol.*, 2009, **23**, 1907.
5 K. E. Jensen, R. Sarfati, R. W. Style, R. Boltyanskiy, A. Chakrabarti, M. K. Chaudhury and E. R. Dufresne, *Proc. Natl. Acad. Sci. U. S. A.*, 2015, **112**, 14490.
6 Z. Cai, A. Skabeev, S. Morozova and J. T. Pham, *Commun. Mater.*, 2021, **2**, 21.
7 P. W. Wilson, W. Lu, H. Xu, P. Kim, M. J. Kreder, J. Alvarenga and J. Aizenberg, *Phys. Chem. Chem. Phys.*, 2013, **15**, 581.
8 A. K. Epstein, T.-S. Wong, R. A. Belisle, E. M. Boggs and J. Aizenberg, *Proc. Natl. Acad. Sci. U. S. A.*, 2012, **109**, 13182.
9 Z. Shao and Q. Liu, *Extreme Mech. Lett.*, 2023, 101996.
10 X. Lou, Y. Huang, X. Yang, H. Zhu, L. Heng and F. Xia, *Adv. Funct. Mater.*, 2020, **30**, 1901130.
11 A. Hourlier-Fargette, A. Antkowiak, A. Chateauminois and S. Neukirch, *Soft Matter*, 2017, **13**, 3484.
12 L. Hauer, Z. Cai, A. Skabeev, D. Vollmer and J. T. Pham, *Phys. Rev. Lett.*, 2023, **130**, 058205.
13 H. Jeon, Y. Chao and S. Karpitschka, *Phys. Rev. E*, 2023, **108**, 024611.
14 W. Qian, W. Zhao, T. Qian and Q. Xu, *Phys. Rev. Res.*, 2024, **6**, 033210.
15 Q. Liu and Z. Suo, *Extreme Mech. Lett.*, 2016, **7**, 27.
16 J. Zhu and Q. Liu, *J. Mech. Phys. Solids*, 2023, **170**, 105124.

 This journal is © The Royal Society of Chemistry 2025

Open Access Article. Published on 25 July 2025. Downloaded on 4/4/2026 1:35:03 PM.
This article is licensed under a Creative Commons Attribution-NonCommercial 3.0 Unported Licence.

17 J. Zhu, C. Yang and Q. Liu, *Soft Matter*, 2023, **19**, 8698–8705.
18 L. Wang and Q. Liu, *Soft Matter*, 2024, **20**, 3676.
19 R. W. Style, A. Jagota, C.-Y. Hui and E. R. Dufresne, *Annu. Rev. Condens. Matter Phys.*, 2017, **8**, 99.
20 B. Andreotti and J. H. Snoeijer, *Annu. Rev. Fluid Mech.*, 2020, **52**, 285.
21 Q. Liu, T. Ouchi, L. Jin, R. Hayward and Z. Suo, *Phys. Rev. Lett.*, 2019, **122**, 098003.
22 A. Chakrabarti and M. K. Chaudhury, *Langmuir*, 2013, **29**, 6926.
23 K. L. Johnson, *Contact mechanics*, Cambridge University Press, 1987.
24 A. A. Günay, S. Sett, Q. Ge, T. Zhang and N. Miljkovic, *Adv. Mater. Interfaces*, 2020, **7**, 2000983.
25 A. Pandey, B. Andreotti, S. Karpitschka, G. Van Zwieten, E. H. van Brummelen and J. H. Snoeijer, *Phys. Rev. X*, 2020, **10**, 031067.
26 R. Masurel, M. Roché, L. Limat, I. Ionescu and J. Dervaux, *Phys. Rev. Lett.*, 2019, **122**, 248004.